Springer

Chinese Society of Pavement Engineering

International Journal of
Pavement Research and Technology

Journal homepage: www.springer.com/42947

Recent advances in characterizing the "bee" structures and asphaltene particles in asphalt binders

Yuhong Wang[a]*, Kecheng Zhao[b], Fangjin Li[a], Qi Gao[c], King Wai Chiu Lai[c]

[a] *Dept. of Civil and Environmental Engineering, The Hong Kong Polytechnic University, Hong Kong SAR, China*
[b] *Zhejiang Communications Construction Group Co., Ltd., Zhejiang Province, China*
[c] *Dept. of Biomedical Engineering, Centre for Robotics and Automation, City University of Hong Kong, Hong Kong SAR, China*

Received 20 November 2020; received in revised form 24 November 2020; accepted 24 November 2020

Abstract

The microscopic surface features of asphalt binders are extensively reported in existing literature, but relatively fewer studies are performed on the morphology of asphaltene microstructures and cross-examination between the surface features and asphaltenes. This paper reports the findings of investigating six types of asphalt binders at the nanoscale, assisted with atomic force microscopy (AFM) and scanning transmission electron microscopy (STEM). The surface features of the asphalt binders were examined by using AFM before and after being repetitively peeled by a tape. Variations in infrared (IR) absorbance at the wavenumber around 1700 cm^{-1}, which corresponds to ketones, were examined by using an infrared s-SNOM instrument (scattering-type scanning near-field optical microscope). Thin films of asphalt binders were examined by using STEM, and separate asphaltene particles were cross-examined by using both STEM and AFM. In addition, connections between the microstructures and binder's physicochemical properties were evaluated. The use of both microscopy techniques provide comprehensive and complementary information on the microscopic nature of asphalt binders. It was found that the dynamic viscosities of asphalt binders are predominantly determined by the zero shear viscosity of the corresponding maltenes and asphaltene content. Limited samples also suggest that the unique bee structures are likely related to the growth of asphaltene content during asphalt binder aging process, but more asphalt binders from different crude sources are needed to verify this finding.

Keywords: Asphalt microstructures; Asphalt aging; Atomic force microscopy; Scanning transmission electron microscopy; Asphaltenes

1. Introduction

Asphalt binder is a highly viscous fluid. Its microscopic nature has been a subject of interest for over a century. As early as in 1914, Rosinger proposes a colloidal structure for asphalt binder [1-2], and the colloidal model is later discussed in detail by Nellensteyn [2-3]. In such a colloidal model, asphaltenes are the key components in the solid phase, with some attached resins serving as peptizing agents [2]. The peptized asphaltenes are suspended in the rest liquid fraction called maltenes. Asphaltenes not only impart the black color to asphalt binder [4] but also play a key role in asphalt binder's rheological properties. More specifically, asphaltenes are the "thickeners" that drive up the viscosity of asphalt binder [4]. For a same type of asphalt binder, increase in asphaltene content is well related to its increase in binder viscosity [5]. For different types of asphalt binder, however, there is no universal relationship between asphaltene content and binder viscosity. This is understandable because according to the colloidal theory, asphalt binder viscosity is determined by both the volume fraction of the solid-phase asphaltenes and the viscosity of the liquid medium—maltenes. The viscosity of maltenes varies from binder to binder, not to mention that asphaltene morphology may also play a role in binder viscosity.

Recent years witness a rising interest in studying the microscopic nature and behaviors of asphalt binders. A noteworthy research area is the use of molecular dynamics (MD) simulation to model and simulate asphalt binder behaviors as well as interactions between asphalt binder and aggregate [e.g., 6-7]. In such endeavors, an average molecular size and composition are usually assumed for the individual fraction (e.g., saturates, aromatics, resin, asphaltenes, SARA) of asphalt binders [8]. The validity of the simulation results, however, is dependent on the accuracy of the assumptions. In addition, the use of average molecules cannot explain large variations in asphalt binder behaviors. In parallel, with the advancement in imaging technologies, various methods have been used to examine the microscopic nature of asphalt binders. A popular approach is the use of atomic force microcopy (AFM), which reveals some interesting surface features of asphalt binders. Perhaps the most notable surface feature is the "bee"

* Corresponding author
E-mail address: yuhong.wang@polyu.edu.hk (Y. Wang).
Peer review under responsibility of Chinese Society of Pavement Engineering.

ISSN: 1997-1400 DOI: https://doi.org/10.1007/s42947-020-6008-3
Chinese Society of Pavement Engineering. Production and hosting by Springer Nature

structure, also known as Catana phase [e.g., 9-11]. Typically, the Catana phase is surrounded by a peri phase, which a separated by a matrix called perpetua phase [11-12]. The nature of the surface feature, particularly the "bee" structure, is subject to many speculations, ranging from asphaltenes [13-14], surface wrinkles [15], crystalline waxes [10] and a combination of different substances and mechanisms [16]. In addition, it is still arguable whether the surface features are exclusive to the surface of the asphalt binder specimens or also present inside the specimens. In addition to AFM, other techniques have also been used to investigate microstructures in asphalt binders, including transmission electron microscopy (TEM) and scanning electron microscopy (SEM) [17].

To date, consensus has not been reached on the nature of nano-scale microstructures in asphalt binders. Yet, bulk nano-scale microstructures, which are supposed to be dominated by asphaltenes, are the key element that underpins the colloidal model of asphalt binders. The purpose of this paper is to present recent research findings on nano-scale characterization of microstructures in asphalt binders, with focus on the use of different imaging technologies. The next section introduces materials and methods used for the investigation. Section three discusses the research findings, while section four summarizes and concludes the paper.

2. Materials and method

A series of investigations were performed to evaluate the microscopic nature of asphalt binders. The materials used for the investigation and some of their chemical properties are shown in Table 1. Four of the virgin asphalt binders were used in the U.S. Strategic Highway Research Program (SHRP), and the other one is a commonly used binder in Hong Kong. The reclaimed asphalt binder was obtained from a field pavement that was used for 36 years before being demolished [18]. Table 1 indicates that binder AAD-1 and AAK-1 are high in the content of surfur and two tested heavy metals. Binder AAM-1 has high wax content.

Different methods were used in this study to examine the "bee" structures and asphaltene particles in asphalt binders. Attempts were also made to connect the microstructures to the rheological properties of asphalt binders. The main methods used in this paper are discussed as follows.

2.1. Examination of surface microstructures and features using AFM and AFM-IR

Three pieces of AFM equipment, all from Bruker, were used to assist in the investigation. The first piece was mainly used to investigate the surface topology and phase contrast of different asphalt binder samples. The asphalt binder samples were deposited on a Mica plate by using heat cast. The probe is made of Si, N-type (AppNano, Model ACTA), with a tip radius less than 10 nm and height between 14 and 16 μm [20]. The second piece (BioScope Catalyst) was used to examine the microstructures in detail, using an AFM RTESPA tip with a radius in the range of 8 nm to 12 nm. An inverted optical microscope was combined to the AFM system to locate and probe the interested objects. The third piece, an s-SNOM instrument, is located at the Bruker lab in Santa Barbara, California. The AFM system uses 40 N/m cantilever, PtIr coated with about 20 nm tip radius. The unique feature of the system is that it integrates with infrared (IR) spectroscopy at the nanoscale so that variations in chemical composition at the sample surface can be explored.

As mentioned previously, bee structures and other surface features of asphalt binders have been extensively investigated by using AFM in existing studies. To examine if the surface features are indeed limited to sample surface or exit in bulk sample, a peeling technique was used to remove the surface features. In performing surface peeling, an adhesive tape was gently applied to the asphalt binder sample. It is anticipated that surface features would be removed by such action and the removal of the surface features would reveal internal microstructures, if there are any. To avoid sample surface irregularity caused by peeling, the sample was heated to 95ºC after peeling before it was reexamined. A total of 5 peeling-heating cycles were performed on the samples, and observations were made after each cycle.

Another method that distinguishes this study from existing ones is the integration of AFM and IR. The formation of asphaltenes in asphalt binder is associated with oxidative aging. Fig. 1 shows the IR spectrum of asphalt binder P60/70 and asphaltenes obtained from the same binder. As shown in the figure, strong absorptions appear at the wavenumber of 1260, 1700, and 3260 cm^{-1}, likely corresponding to the chemical bond of C-O, C=O, and O-H, respectively [21]. The Bruker s-SNOM system is capable of simultaneously generating the surface IR diagram at the nano-scale

Table 1
Basic information and chemical properties of asphalt binders (*Data before the bracket is the high-temperature PG grade of the binder tested in the SHRP program, while data in the bracket is grade determined in this study) [19].

Binder information	Binder type					
	Virgin					Reclaimed
	AAD-1	AAG-1	AAK-1	AAM-1	P60/70	P80/100R
Oil source	Ca Coast	Ca Valley	Boscan	W Tx Inter	Middle East	Middle East
PG grade	58(64)*-28	58(70)-10	64(64)-22	64(64)-16	64-16	Unknown Penetration grade: 80-100
C, %	81.6	85.6	83.7	86.8		
S, %	6.9	1.3	6.4	1.2		
Vanadium, ppm	310	37	1480	58		
Nickel, ppm	145	95	142	36		
Aromatic C%	23.7	28.3	31.9	24.7		
Aromatic H%	6.82	7.27	6.83	6.52		
Wax, %	1.94	1.13	1.17	4.21	1.6	--

in

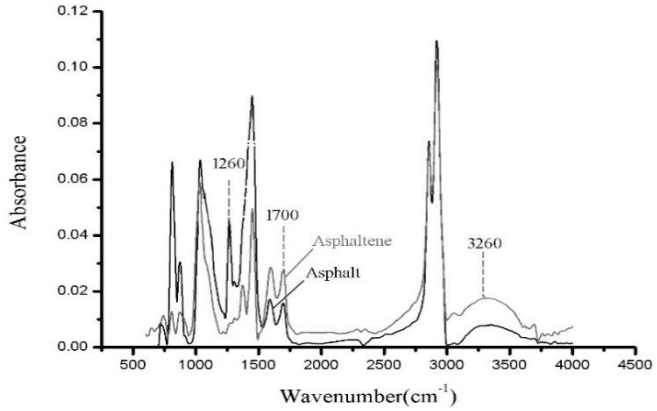

Fig. 1. The FTIR spectrum of asphaltenes and asphalt binder.

conjunction with the diagrams of surface topography, phase, modulus, adhesion, and deformation. This research component aims to evaluate if the absorbance at the wavenumber around 1700 cm^{-1} (characteristic IR absorption for Ketone, C=O) is related to any surface features. If positive relationship is found, it would indicate that the surface feature is rich in asphaltene content.

2.2. *Examination of internal microstructures using STEM and cross-examination of microstructures using STEM and AFM*

A large number of samples were also evaluated by using a scanning transmission electron microscopy (STEM)—Field Emission Electron Microscope STEM (JEOL Model JEM-2100F). In using TEM or STEM, a beam of electrons needs to be transmitted through a thin specimen in order to generate an image. TEM provides several advantages. Firstly, the resolution of TEM image can be as high as less than 1 nm. Secondly, because the electrons penetrate the samples, TEM images reveal the internal details of the samples. Thirdly, other analytical instruments such as EDS (Energy Dispersive X-ray Spectrometer) can be integrated with the system for chemical analysis of the samples.

On the other hand, TEM or STEM has its limits. Firstly, the samples have to be very thin to enable electrons to pass, usually in the range of hundreds of nanometers or even less. In early attempts, the authors used solvent casting to create thin films for the observation of asphalt binders and asphaltenes in STEM [17]. In later experiments, the authors developed a new method to create thin films without solvent casting. Secondly, TEM images are formed due to material property variations (e.g., density) or large thickness difference. Surface features in asphalt binders that vary little in height but without density difference cannot be seen in STEM. The density of asphaltene particles is about 1.15 g/cm^3, which is heavier than the maltene phase (about 1 g/cm^3). Therefore, asphaltene particles may be more easily distinguished than others such as those made of wax. Thirdly, it is difficult to create a three-dimensional view of an object based on TEM images. In previous studies by the authors [17], STEM has been successfully used in characterizing asphaltene particles in asphalt binders. This paper will only briefly introduce some major findings from STEM studies. The experimental details and findings will not be elaborated.

Instead, this paper will be more focused on the cross-examination of microstructures by using both STEM and AFM. For this purpose, the authors created marks on the sample placed on the TEM grid. The same sample was also used for examination using AFM, and the marks assist in finding the interested region. For illustration purpose, a marked asphalt film sample used for both STEM and AFM examinations are shown in Fig. 2. In addition, asphaltene particles were cross-examined by using both STEM and AFM. Cross-examination not only helps verify the nature of particles found in STEM and AFM images, but also helps reveal possible relationships between them.

2.3. *Aging treatment and rheological tests*

While the images of "bee" structures and asphaltene articles shed lights on the surface or internal morphologies of asphalt binders, from the perspective of engineering applications, one would concern more about the impacts of such microstructures on the macro properties of asphalt binders. This research component aims to investigate the underlying factors that determine the rheological properties of asphalt binder, using the dynamic viscosity of the tested asphalt binders as an indicator.

In a related study, the five types of virgin asphalt binders used in this study were subject to long-term aging treatments under three conditions, after being short-term aged by using a rolling thin film oven (RTFO). In the first condition, the binder was aged at 60°C in an unpressurized, dark chamber for 6, 12, 15 and 18 months. In the second condition, the asphalt binder samples were aged in an autoclave filled with pressurized pure oxygen of 0.5 mPa at a target temperature of 70°C. The aging periods were chosen to be 14, 21, 28 days, respectively. In the third condition, the binder samples were aged in a pressure aging vessel (PAV) at 100°C in accordance with ASTM D6521 for 20, 40 and 60 hours, respectively. A total of 60 asphalt binder samples were generated and used for study. The purpose of the existing study was to evaluate if different aging conditions lead to different physicochemical properties of long-term aged asphalt binders [22].

In this paper, test data obtained in the previous study was re-analyzed to evaluate factors that affect binder's dynamic viscosity, which is obtained from the oscillation shear test using a dynamic shear viscometer (DSR) by the following equation:

$$\eta' = \frac{G''}{\omega} \tag{1}$$

where, $\eta'$is the dynamic viscosity (Pa.s) of the asphalt binder, G'' is the loss modulus (Pa), and ω is loading frequency (rad/s).

In this study, data obtained at the temperature of 64°C and angular frequency of 9.96 rad/s were used, except for binder AAG for which the test temperature was chosen to be 52°C due to the softness of the binder.

The asphalt binders were separated into asphaltenes and maltenes according to the Corbett fraction procedure, but the maltene phase was not further separated into saturates, aromatics and resins. The maltene phase was tested to obtain its zero shear

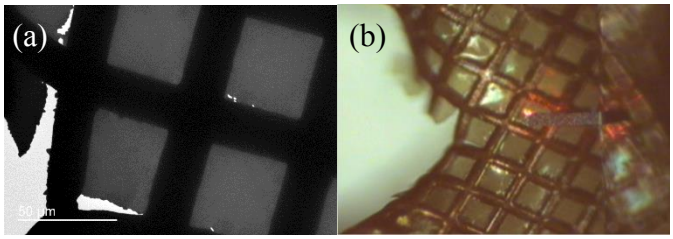

Fig. 2. The cross-examination of asphalt microstructures using TEM and AFM by marking the specimen on TEM (a) Marked asphalt binder specimen examined under TEM and (b) The same specimen examined under AFM.

viscosity (ZSV) by rotational test using the Carreau-Yasuda equation [23]:

$$\frac{\eta(\dot{\gamma})-\eta_\infty}{\eta_0-\eta_\infty} = \frac{1}{(1+(\lambda\cdot\dot{\gamma})^{\frac{1-p}{p_1}}} \quad (2)$$

where, $\dot{\gamma}$ is the shear rate, η_0 is the zero shear viscosity, η_∞ is the infinite-shear viscosity, λ is the relaxation time, p_1 is the "Yasuda exponent", and p is the "power-law-index": $p < 1$ for shear-thinning, $p > 1$ for shear-thickening, $p = 1$ for ideally viscous flow behavior.

In the rotational test for maltenes, the shear rate $\dot{\gamma}$ was set to change from 0.1 to 100 1/s. The fitting of measured data to the Carreau-Yasuda equation and the calculation of η_0 was performed by the RheoCompass™ Software. Fig. 3 shows the ZSV values of maltenes obtained from the five types of binders. As can be seen in the figure, the ZSV values of the maltenes vary greatly with binder source. For instance, the ZSV of maltenes from binder AAM is 45 times greater than the ZSV of maltenes from binder AAD.

The ratio between the dynamic viscosity of asphalt binder and that of the corresponding maltene phase was used to eliminate the effect of maltenes and evaluate the effects of particulate phase. However, data on the dynamic viscosity of maltenes (ω=9.96 rad/s) is not available. Therefore, the ratio of between the dynamic viscosity of asphalt binder and the ZSV of the corresponding maltene phase was used. Fig. 4 shows the rotational viscosity of maltenes from two example asphalt binders. The figure indicates that, at a same test temperature, the viscosity of maltenes is not sensitive to changes in shear rate. Therefore, using ZSV instead of the dynamic viscosity of maltenes to calculate the ratio is also reasonable.

3. Results and discussion

3.1. Changes in the surface features of asphalt binders

The surface features of the five virgin asphalt binders are shown in Fig. 5. For each binder, the left side shows the topography while the right side shows the phase diagram. In addition, the surface features of both the original binders and those after being peeled for five times are shown in the Figure.

Fig. 5 indicates that the surface features vary with binder type. For binder P60/70, the "bee" structures are noticeable, but the number is relatively scare and the size is small. For binder AAD-1 and AAK-1, the "bee" structures are extensive and in larger size. For binder AAG-1 and AAM-1, there are no noticeable "bee" structures: The sample surface appears to be very smooth. The intensity of the bee structures follows the order of AAD-1≅AAK-1>P60/70>AAG-1=AAM-1. Note that the surface morphologies of binder AAD-1, AAK-1, AAG-1 and AAM-1 are similar to those of the same binders reported by Pauli et al [10]. Pauli et al. [10] conclude that the bee structures are attributed to the interactive effects between crystalizing paraffin waxes and asphalt components. The wax contents of the three types of binders are shown in Table 1, which indicates that the total wax content may not correlate with the surface features. Moreover, an existing study found that the dewaxing procedure also causes the removal of asphaltenes [20].

As shown in Fig. 5, most of the surface features can be removed after repetitive peeling by using a tape. After being peeled, the surfaces of the specimens generally become quite smooth. This

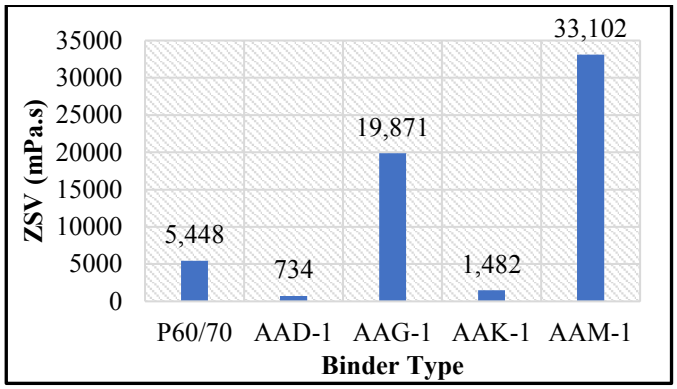

Fig. 3. The ZSV (mPa.s) values of maltenes derived from the five types of asphalt binders (64ºC) .

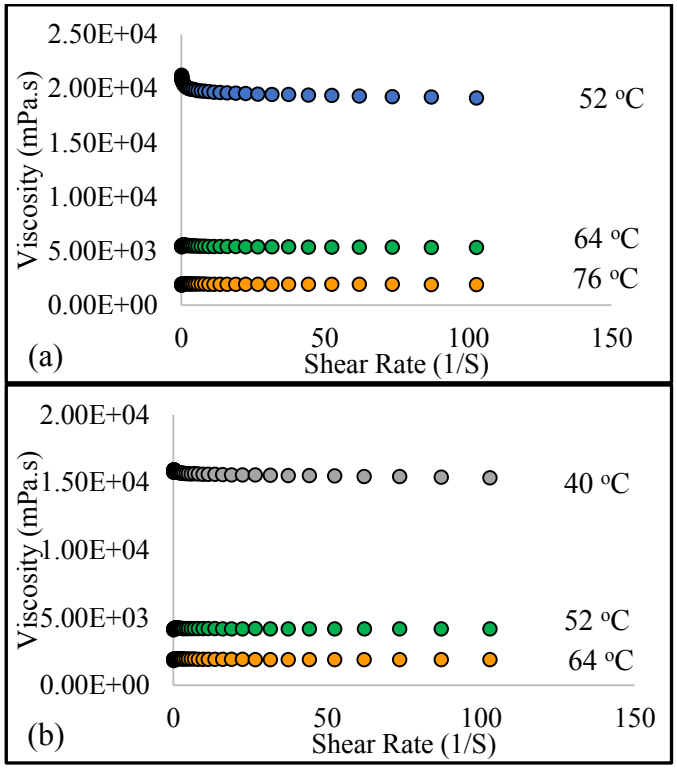

Fig. 4. Examples of changes in maltene viscosity with temperature and shear rate (a) P60/70 and (b) AAK-1.

suggests that the features are mainly a surface phenomenon, which may not heavily affect the bulk binder properties. However, even after repetitive peeling, the phase diagrams still show some contrasts, likely associated with material property variations.

3.2. Relationships between surface features and NanoIR absorption

The images of topography (left) and nanoIR absorption (right) of four out of six examined specimens are shown in Fig. 6. For each binder type, both the topography and nanoIR absorption before and after being peeled are shown in the figure. The other two specimens are not shown because they are prepared by solvent casting, which left circular depressions on the specimen surface that likely interfere the surface images and IR results. It is

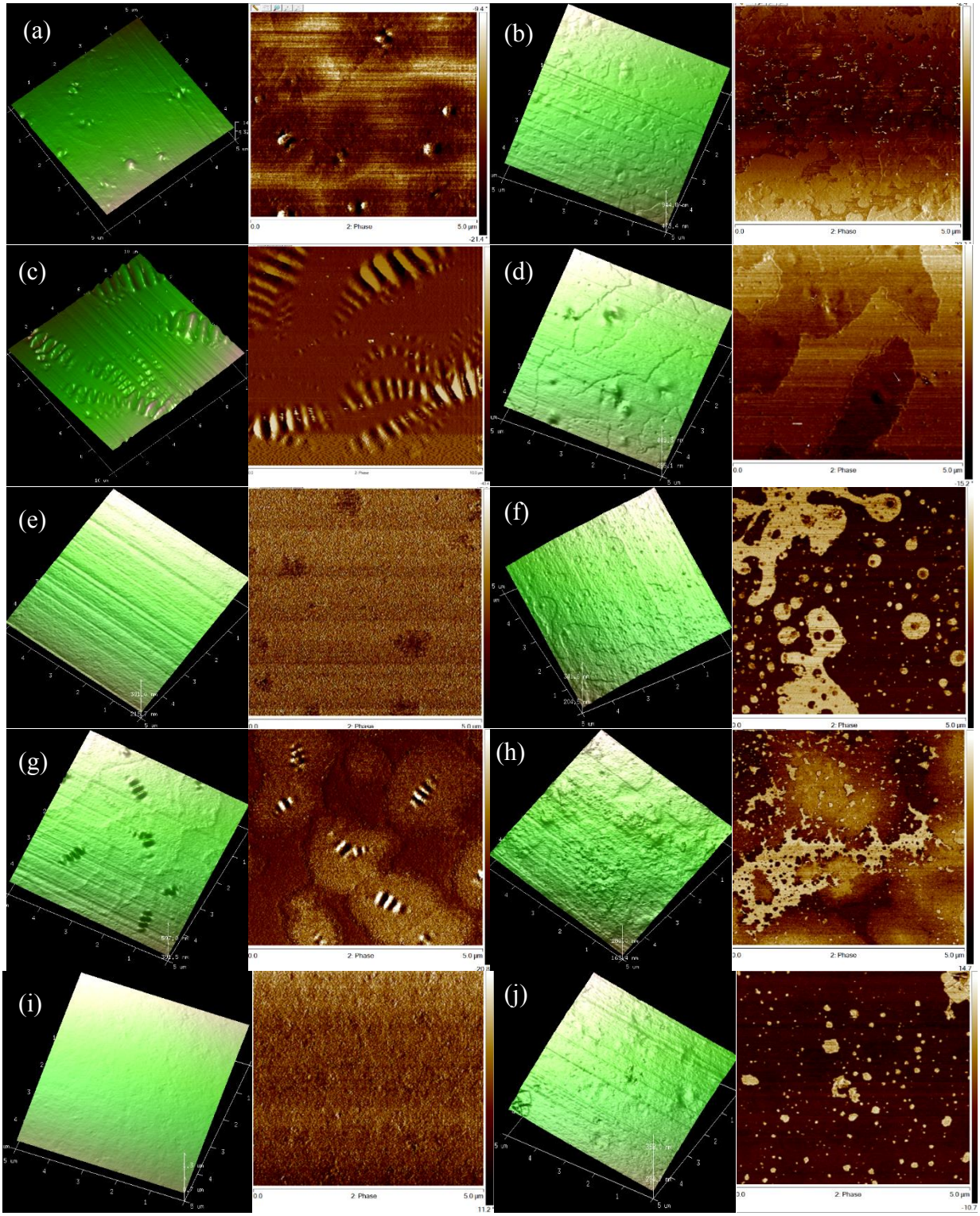

Fig. 5. The topography and phase diagrams of five asphalt binders: before and after surface peeling (a) P60/70: Original, (b) P60/70: After peeling, (c) AAD-1: Original, (d) AAD-1: After peeling, (e) AAG-1: Original, (f) AAG-1: After peeling, (g) AAK-1: Original, (h) AAK-1: After peeling, (i) AAM-1: Original, and (j)AAM-1: After peeling.

interesting to note that binder AAD-1 did not show bee structures immediately after being peeled in the middle of July 2015. After it was sent to the Bruker's lab in California and tested in November 2015, some bee structures reappear on the sample surface. However, the peeled bee structures did reappear on the sample surface of reclaimed asphalt binder.

The images of nanoIR absorption obtained with an s-SNOM instrument appear to be not related to any surface features.

Although there are some regions with high intensity of IR absorption, the regions are not limited to those bee structures. The reclaimed asphalt binder also shows some contrasts in IR absorption, but the contrasts seem more related to the height of the sample surface. Overall, the NanoIR absorption images do not reveal a clear pattern of IR on the sample surface, implying that none of the features are related to high concentration of asphaltenes.

3.3. STEM images

STEM images have been taken for all the samples. Systematic comparisons of STEM images of asphalt binders of different aging states are provided in another r paper [24], hence they are not repeated here. Instead, only STEM images corresponding to three asphalt binders in Fig. 5 are shown in Fig. 7 for reference purpose. Note that the circular features in the images are just holes in the carbon support films on copper grids.

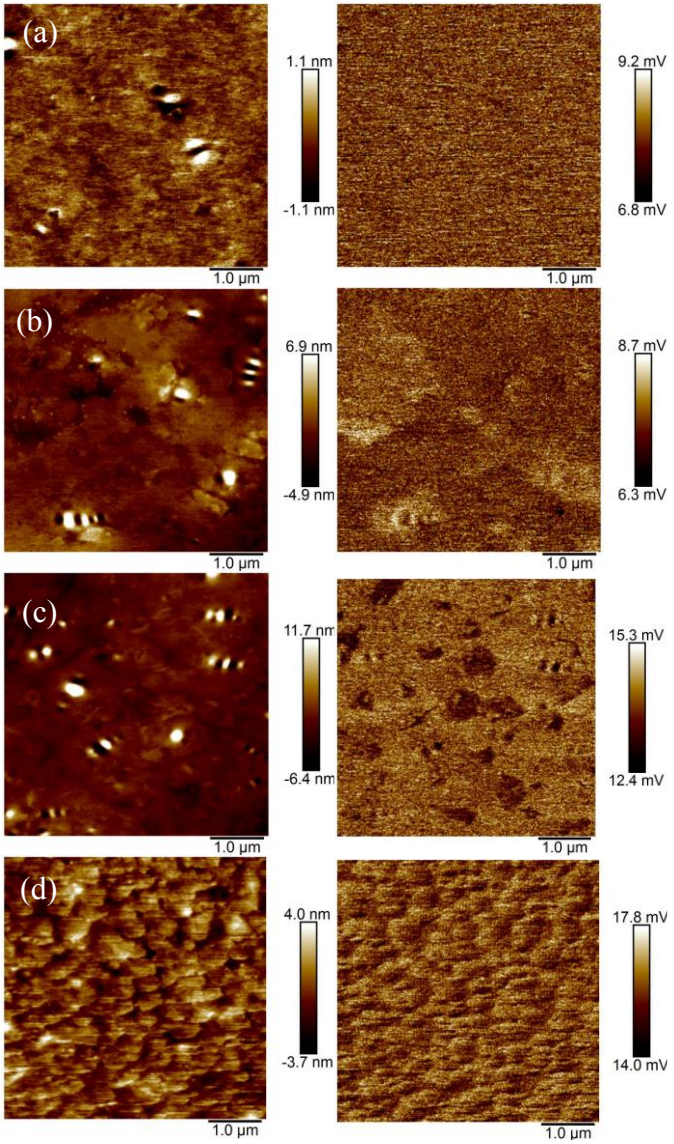

Fig. 6. The topography and nanoIR diagrams of selected specimens: before and after surface peeling (a) AAD-1: topography and nanoIR (original binder after resting for 4 months), (b) AAD-1: topography and nanoIR (after peeling and resting for 4 months), (c) P80/100R: topography and nanoIR (after resting for 4 months), (d) P80/100R: topography and nanoIR (after peeling and resting for 4 months).

It is clear in Fig. 7 that the STEM images are quite different than those AFM images. In particular, bee structures cannot be found in TEM images. For non-aged asphalt binders, the microstructures (black dots in the images) are generally small, but the grain size and morphology of the microstructures vary with binder type as well as in different regions of the same specimen. For example, more noticeable microstructure agglomeration can be found in some regions of binder AAM-1. Based on the analysis of asphalt binders from different sources, one existing paper attributes those microstructures to asphaltenes [17].

As asphalt binder ages, obvious changes can be found in the morphologies of microstructures in the STEM images. Fig. 8 shows the microstructures in asphalt binder AAD-1 after being aged in RTFO and PAV. As compared with non-aged binder, noticeable increased associations can be found among the microstructures. As marked in Fig. 8(a), some microstructures are aligned to form agglomerates of greater size. As asphalt binder is further aged in a PAV, dramatic changes further occur inside of the asphalt binder. The most noticeable change is the formation of needle-shaped (or rod-like) crystalline microstructures, with size varying from tens of nanometers to more than 1 μm. In addition, other irregularly shaped microstructures can also be found. It is evident that aging not only causes increases in asphaltene content but also changes in the associations of asphaltenes. Such changes cannot be revealed in the AFM images in Fig. 5 and Fig. 6.

The separately asphaltene microstructures have been examined and discussed in detail in an existing paper [17]. For the interest of completeness, one of such microstructures in a larger size and the details of a needle-shaped microstructure are shown in Fig. 9. The microstructure in Fig. 9(a) was created by dissolving reclaimed asphalt binder in Tetrahydrofuran (THF). As shown in Fig. 9(a), this needle-shaped asphaltene microstructure appears to be very regular in shape. It is difficult to examine such microstructures in greater detail in TEM as they are susceptible to decomposition by radiative damages. Nevertheless, Fig. 9(b) reveals some details of a decomposing microstructure. Stacks of well-ordered layered structure can be seen in Fig. 9(b). Each layer is likely to be an individual asphaltene molecule's aromatic sheet, which is stacked together similar to the structure of graphite.

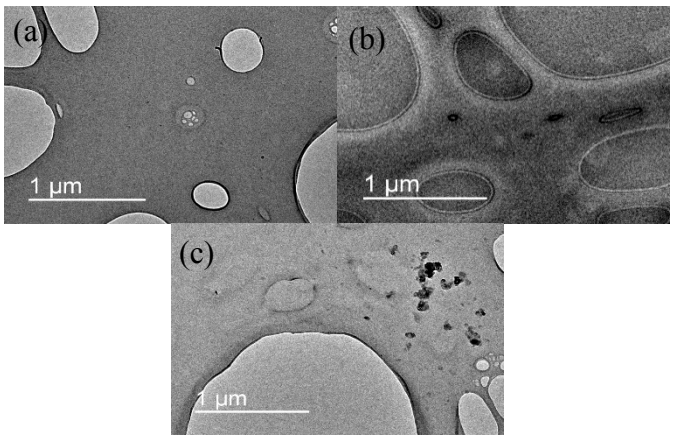

Fig. 7. Representative STEM images of three types of asphalt binders (a) AAD-1, (b) P60/70, (c) AAM-1.

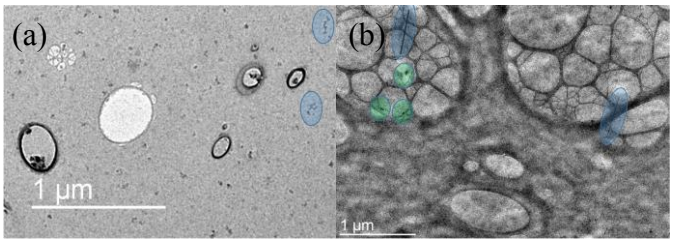

Fig. 8. Changes in asphaltene microstructures after asphalt binder being aged in RTFO and PAV. (a) AAD-1 after RTFO treatment and (b) AAD-1 after PAV treatment.

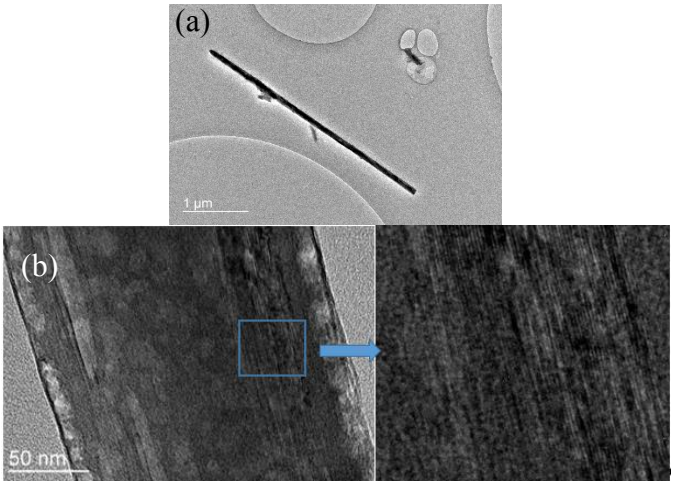

Fig. 9. Details of needle-shaped asphaltene microstructures (a) A needle-shaped asphaltene particle (b) Details of a needle-shaped asphaltene particle.

3.4. *Cross examination of bee structures and asphaltene particles in AFM and STEM*

Although the bee structures, unlike asphaltene particles, cannot be seen in TEM images, it would be interesting to examine if they co-exist or if there are any associations between the two types of particles. Thanks to the techniques of creating a thin film of asphalt binder without solvent casting and accurately marking the STEM grid (Fig. 2), one can create a thin film of asphalt binder, mark a region with identified asphaltene particles, and examine the specimen surface using AFM.

The STEM image and AFM image of a thin asphalt binder specimen in the same region are shown in Fig. 10. Also shown in the figure are the topography and phase diagram of the thin specimen surface and the surface profiles of the asphaltene particles and bee structures at selected locations.

Asphaltene particles of different morphologies can be seen in the STEM image of the asphalt binder, which is extracted from field-aged asphalt. The 3D specimen surface in Fig. 10(b) reveals that one asphaltene particle is protruded from the specimen surface and there are several noticeable bee structures. Large asphaltene particles and bee structures can indeed co-exist on asphalt binder sample surface, if the surface is thin enough (about hundreds of nanometers). The surface profiles of the asphaltenes and the bee structures indicate that the specimen's surface irregularity caused by the asphaltene particle is much greater than that caused by the bee structure. In addition, the surface of the asphaltene particles appears to be very smooth along the longitudinal direction.

Both the topography and phase diagram indicate that one bee structure is connected to the asphaltene particle. The connection may be just coincidence, because there are also isolated bee structures. The phase diagram indicates that the phase of the asphaltene microstructure is similar to the phase corresponding to the peaks of the bee structure. This indicates that their interaction with the AFM tip is more similar as compared with the other regions, where maltenes are mixed with small-size asphaltenes.

The needle-shaped asphaltene particle was examined in detail in AFM and shown in Fig. 11. Although layered structure can be detected on the surface of the asphaltene particle, the surface appears not uniform: the layered structure is more predominant in certain regions than in others. In addition, the detailed view of the layered structure indicates that there are extensive crosslinks between the apparent layers. The images reveal the heterogeneous nature of the asphaltene particle.

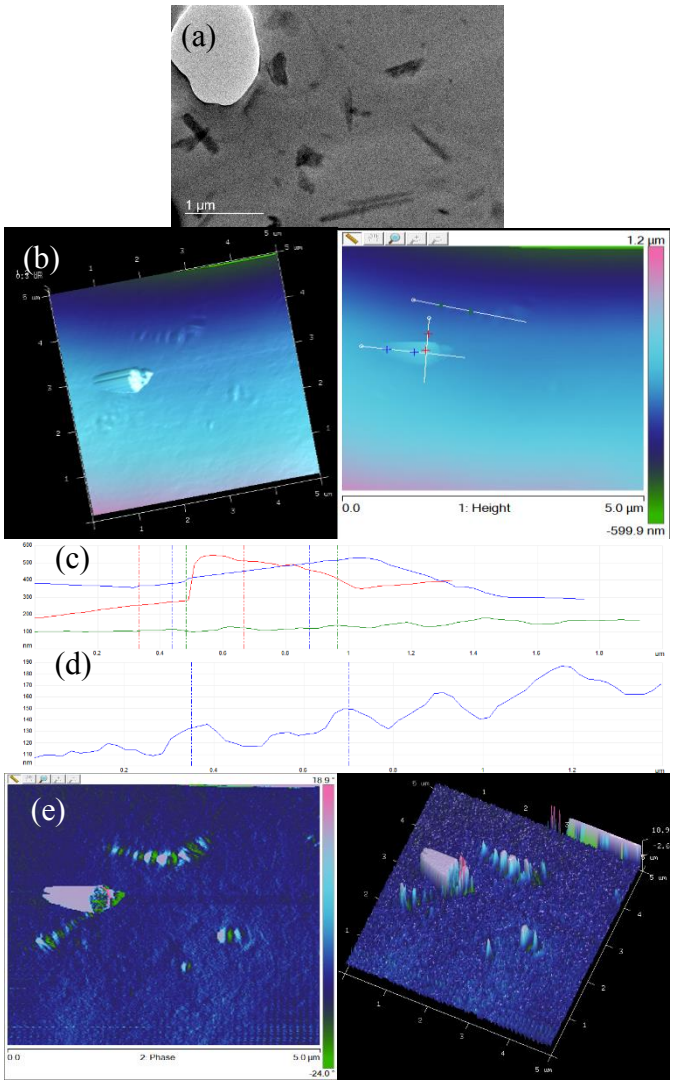

Fig. 10. Cross-examination of asphaltene particles and bee structures in STEM and AFM images (a) The region of the STEM image selected for observation under AFM, (b) The AFM image of the selected region, (c) The topography of a protruded asphaltene particle and a bee structure, (d) The topography of the bee structure, (e) The phase diagram of the asphaltene particle and bee structures.

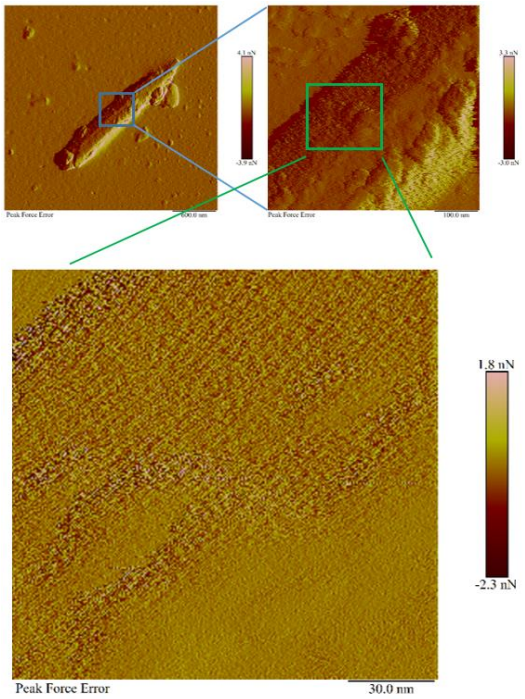

Fig. 11. The detailed examination of asphaltene particles in AFM.

3.5. *The key role of asphaltenes*

Pavement engineers may be more interested in the impacts of the bee structures and asphaltene particles on the engineering properties of asphalt binders. As mentioned before, five types of asphalt binders were aged to different extent and tested for dynamic viscosity. The ZSV of maltenes separated from the corresponding non-aged asphalt binders were also tested. Relationships between asphaltene content and the viscosity ratio (dynamic viscosity of binder/ZSV of maltenes of the binder at the same temperature) are shown in Fig. 12. Several observations can be made in the figure.

Firstly, in spite of being derived from different crude oil source and being treated by different conditions (PAV, pressurized pure oxygen, and long-term aging in an atmospheric pressure), there is a remarkably good universal relationship between asphaltene content and the viscosity ratio. This suggests that the viscosity of asphalt binders is essentially determined by the viscosity of maltenes and the fractions of the particle phase—asphaltenes. This also implies that the ZSV of the maltene phase does not change largely as asphalt binder ages, because the ZSV of maltenes form non-aged asphalt binders are used to calculate the viscosity ratio. The figure suggests that asphalt binder is best modelled as a colloidal system, in which the volume fraction of solid phase and viscosity of the liquid medium determine the system viscosity. A limit in Fig. 12 is that the proportion of resins attached to asphaltenes cannot be quantified, but it seems not greatly affecting the relationship between the volume of solid phase and viscosity ratio.

By assuming a wax density of 0.9 g/cm^3, relationship between the combined asphaltene and wax content and the viscosity ratio is shown in Fig. 13. As can be seen, the coefficient of determination (R^2) drops after counting the wax content. The deviation from the log-linear relationship is more obvious for binder AAM-1, which has a high wax content of 4.21% (Table 1). The regression result suggests that wax does not significantly and positively contribute to increase in asphalt binder's dynamic viscosity. Except for binder AAG-1, for which the dynamic viscosity was tested at 52°C, all the other binders' dynamic viscosity was tested at 64°C. It is also possible that some wax was melted at such temperature, which affects their role in the colloidal system.

It is also shown in Fig. 12 that the initial and final asphaltene contents of the asphalt binders after aging vary with binder type. The quantitative changes in asphaltene contents of the binders are shown in Fig. 14, which displays the asphaltene contents in non-aged binder, the maximum asphaltene content after different aging treatments, and the difference between the two.

As shown in Fig. 14, the initial asphaltene content of binder AAK-1 is higher than that of binder P60/70, which is higher than that of binder AAD-1. However, the maximum asphaltene content of AAK-1 is higher than that of AAD-1, which is higher than that of P60/70. In terms of the difference between the initial asphaltene content and the maximum asphaltene content, the order is: AAD-1>AAK-1>P60/70>AAM-1>AAG-1. It seems that AAD-1 is the most susceptible to aging in terms of asphaltene growth. Interesting, this order of asphaltene formation (difference between the initial and maximum) is well related to the order of the intensity of bee structures shown in Fig. 5. It is reasonable to suspect that the bee structure is related to likelihood of asphaltene formation. However, more samples are needed to prove this assumption.

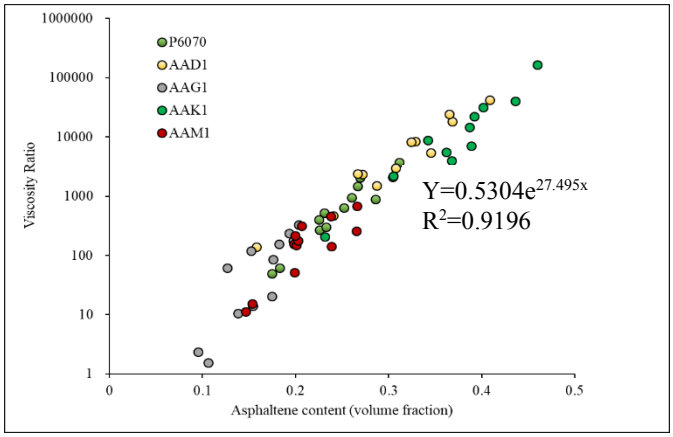

Fig. 12. Relationship between asphaltene content and asphalt binders' viscosity ratios.

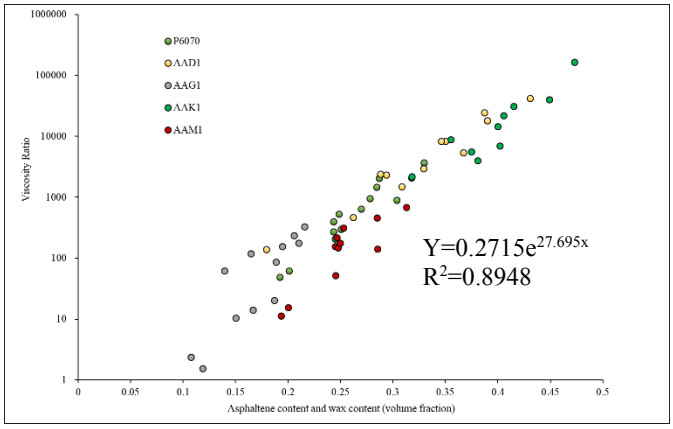

Fig. 13. Relationship between asphaltene plus wax content and asphalt binders' viscosity ratios.

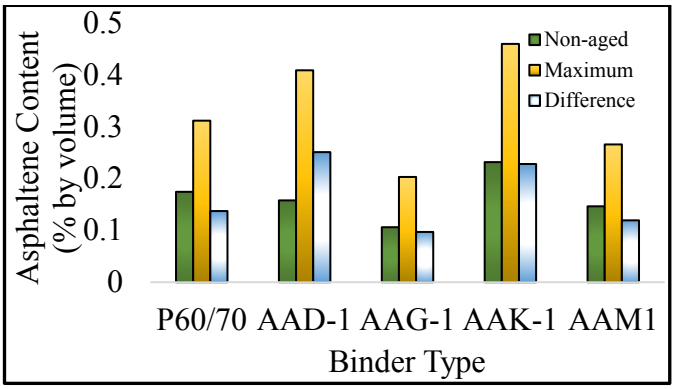

Fig. 14. The initial and largest asphaltene content after artificial aging.

4. Summary and conclusion

Five types of virgin asphalt binders and one reclaimed one were studied for their surface and internal microstructures at the nanoscale, using AFM and STEM, respectively. The surface features of the asphalt binders were examined by using AFM before and after they were repetitively peeled by a tape. Variations in IR absorbance at the wavenumber around 1700 cm^{-1}, which corresponds to ketones, were examined by using an infrared s-SNOM instrument (scattering-type scanning near-field optical microscope). Thin films of asphalt binders were examined by using STEM, and separate asphaltene particles were cross-examined by using both STEM and AFM. The use of both microscopy techniques provide comprehensive and complementary information on the microstructures in asphalt binders. In addition, connections between the microstructures and binder's physicochemical properties were evaluated. The following conclusions are drawn as a result of the investigation:

1. The abundance and existence of bee structures are dependent on binder type, and the bee structures can be removed by surface peeling.
2. Neither original asphalt binder specimens nor those after surface peeling show obvious contrast in surface IR diagram at the selected wavenumber that corresponds to ketones.
3. Asphaltene particles are different with bee structures in morphology, and both can co-exist on a thin asphalt binder surface.
4. The morphology of asphaltene particles is dependent on asphalt binder type and its aging state.
5. Both STEM and AFM images indicate that the needle-shaped asphaltene particles are made of stacked sheets, and the AFM image further reveals crosslinks between the stacked sheets.
6. The ratio between asphalt binder's dynamic viscosity and maltenes' zero shear viscosity is mainly determined by asphaltene content, despite binder source, aging states, and aging treatment methods.
7. Limited samples in this study suggest that the abundance of bee structures are related to the aging susceptibility of asphalt binders in terms of growth in asphaltene content under the same aging conditions.

The methods of examining asphalt microstructures may be used to evaluate aging susceptibility [25] and rejuvenation of asphalt binders [26]. The identified relationship between binders' rheological properties and the rheological properties of maltenes and asphaltene content may be later used for the assessment of blended asphalt [27],

Acknowledgment

This paper is based on the research project (Project No. PolyU 152092/17E) funded by the Research Grant Council of Hong Kong Special Administrative Region Government and the research project (Project Number: 51678510) funded by The National Natural Science Foundation of China (NSFC). The authors would like to thank Bruker for helping test the IR absorbance of the samples.

Reference

[1] A. Rosinger, Beiträge zur Kolloidchemie des Asphalts, Kolloid-Z 15 (5) (1914) 177–179.
[2] D. Lesueur, The colloidal structure of bitumen: Consequences on the rheology and on the mechanisms of bitumen modification, Adv. Colloid Iterface Sci. 145 (1-2) (2009) 42-82.
[3] F.J. Nellensteyn, Bereiding en Constitutie van Asphalt, (Ph. D. Thesis). Delft University, Netherland, 1923.
[4] J.C. Petersen, A review of the fundamentals of asphalt oxidation: chemical, physicochemical, physical property, and durability relationships, Transp. Res. E-Circular. (E-C140) (2009).
[5] Y. Wang, Y. Wen, K. Zhao, D. Chong, J. Wei, Connections between the rheological and chemical properties of long-term aged asphalt binders, J. Mater. Civ. Eng. 27 (9) (2015) 04014248.
[6] A. Bhasin, R. Bommavaram, M. L. Greenfield, D. N. Little, Use of molecular dynamics to investigate self-healing mechanisms in asphalt binders, J. Mater. Civ. Eng. 23 (4) (2011) 485-492.
[7] L. Chu, L. Luo, T. F. Fwa, Effects of aggregate mineral surface anisotropy on asphalt-aggregate interfacial bonding using molecular dynamics (MD) simulation, Constr. Build. Mater. 225 (2019) 1-12.
[8] D. D. Li, M. L. Greenfield, Chemical compositions of improved model asphalt systems for molecular simulations, Fuel 115 (2014) 347-356.
[9] A. Jäger, R. Lackner, C. Eisenmenger-Sittner, R. Blab, Identification of microstructural components of bitumen by means of atomic force microscopy (AFM), PAMM:

Proceedings in Applied Mathematics and Mechanics, WILEY-VCH Verlag, Berlin, 4 (1) (2004) 400-401.
[10] A.T. Pauli, R.W. Grimes, A.G. Beemer, T.F. Turner, J.F. Branthaver, Morphology of asphalts, asphalt fractions and model wax-doped asphalts studied by atomic force microscopy, Inter. J. Pavement Eng. 12 (4) (2011) 291-309.
[11] D. Ganter, S. Franzka, V. V. Shvartsman, D. C. Lupascu, The phenomenon of bitumen 'bee' structures–bulk or surface layer–a closer look, Inter. J. Pavement Eng. (2020) https://doi.org/10.1080/10298436.2020.1823390
[12] H. Fischer, H. Stadler, N. Erina, Quantitative temperature-depending mapping of mechanical properties of bitumen at the nanoscale using the AFM operated with PeakForce TappingTM mode, J. Microscopy 250 (3) (2013) 210-217.
[13] L. Loeber, O. Sutton, J. Morel, J.M. Valleton, G. Muller, New direct observations of asphalts and asphalt binders by scanning electron microscopy and atomic force microscopy, J. Microscopy. 182 (1) (1996) 32-39.
[14] A. Jäger, R. Lackner, C. Eisenmenger-Sittner, R. Blab, Identification of four material phases in bitumen by atomic force microscopy, Road Mater. Pavement Des. 5 (Suppl. 1) (2004) 9-24
[15] Å.L. Lyne, V. Wallqvist, M.W. Rutland, P. Claesson, B. Birgisson, Surface wrinkling: the phenomenon causing bees in bitumen, J. Mater. Sci. 48 (20) (2013) 6970-6976.
[16] X. Yu, N.A. Burnham, M. Tao, Surface microstructure of bitumen characterized by atomic force microscopy, Adv. Colloid Interface Sci. 218 (2015) 17-33.
[17] Y. Wang, K. Zhao, Different forms of asphaltene microstructures discovered in transmission electron microscopy, J. Mater. Civ. Eng. 28 (11) (2016) 04016137.
[18] Y. Wang, Y. Wen, K. Zhao, D. Chong, A.S. Wong, Evolution and locational variation of asphalt binder aging in long-life hot-mix asphalt pavements, Constr. Build. Mater. 68 (2014) 172-182.
[19] D.R. Jones, SHRP materials reference library: Asphalt cements: A concise data compilation (Vol. 1), Strategic Highway Research Program, National Research Council Washington DC, USA, 1993.
[20] Y. Wang, K. Zhao, Analysis of nanoscale microstructures in asphalts of different aging states, J. Mater. Civ. Eng. 28 (1) (2016) 04015090.
[21] Merck KGaA, IR Spectrum Table. (Merck, 2020), https://www.sigmaaldrich.com/technical-documents/articles/biology/ir-spectrum-table.html. Accessed on 19 November 2020.
[22] K. Zhao, Y. Wang, F. Li, Influence of ageing conditions on the chemical property changes of asphalt binders, Road Mater. Pavement Des. (2019) https://doi.org/10.1080/14680629.2019.1637771.
[23] T. G. Mezger, The rheology handbook: for users of rotational and oscillatory rheometers, 4th. Vincentz Network GmbH & Co KG, Hannover, Germany, 2014.
[24] Y. Wang, K. Zhao, Q. Gao, K. W. C. Lai, Asphaltenes in asphalt: Direct observation and evaluation of their impacts on asphalt properties, Constr. Build. Mater. (Under review). (2020).
[25] L. Devulapalli, S. Kothandaraman, G. Sarang, A review on the mechanisms involved in reclaimed asphalt pavement. Inter. J. Pavement Res. Technol. 12 (2) (2019) 185–196.
[26] L. D. Prashanth, N. Palankar, A.U. R. Shankar, A study on the effect of rejuvenators in reclaimed asphalt pavement based stone mastic asphalt mixes. Inter. J. Pavement Res. Technol. 12 (1) (2019) 9–16.
[27] P. Cong, B. Chen, H. Zhao, Coupling effects of wasted cooking oil and antioxidant on aging of asphalt binders. Inter. J. Pavement Res. Technol. 13 (1) (2020) 64–74.